JOURNAL OF GEOPHYSICAL RESEARCH, VOL. 94, NO. C7, PAGES 9761–9778, JULY 15, 1989

Extracting Ocean Surface Information From Altimeter Returns: The Deconvolution Method

ERNESTO RODRÍGUEZ AND BRUCE CHAPMAN

Jet Propulsion Laboratory, California Institute of Technology, Pasadena

We present an evaluation of the deconvolution method for estimating ocean surface parameters from ocean altimeter waveforms. We show that this method presents a fast, accurate way of determining the ocean surface parameters from noisy altimeter data. Three parameters may be estimated by using this method: the altimeter height error, the ocean surface standard deviation, and the ocean surface skewness. By means of a Monte Carlo experiment, we determine an "optimum" deconvolution algorithm and the accuracies with which the above parameters may be estimated using this algorithm. We then examine the influence of instrument effects, such as errors in calibration and pointing angle estimation, on the estimated parameters. Finally, we use the deconvolution algorithm to estimate height and ocean surface parameters from Seasat data.

1. INTRODUCTION

In addition to height information, the return signal of an ocean altimeter contains information about the ocean significant wave height (SWH), the ocean surface skewness, and the scattering cross-section. The emphasis of past altimeters, such as the Seasat and Geosat altimeters, was to obtain rough on-board height, SWH, and wind speed estimates and to apply subsequent corrections based on look-up tables during ground processing. On account of the limitations imposed by the speed of computation, the on-board algorithms used for estimating these parameters had to be very simple. Unfortunately, what was gained in computational efficiency had to be sacrificed in the accuracy and number of the estimated parameters. Thus these two altimeters could not estimate the ocean surface skewness, and the algorithms used to estimate the height suffered biases which were a function of the SWH and the ocean surface skewness [*Born et al.*, 1982; *Hayne and Hancock*, 1982; *Barrick and Lipa*, 1985].

With the advent of cheaper and faster computers, however, one can envisage the implementation of more sophisticated algorithms which will estimate the SWH, skewness, and altimeter height with higher accuracy and in real time. One such algorithm, the deconvolution of the specular point probability density function (pdf), has been advocated by *Priester and Miller* [1979] and Lipa and Barrick [*Lipa and Barrick*, 1981; *Barrick and Lipa*, 1985] and refined by one of us [*Rodríguez*, 1988]. The idea behind this algorithm is as follows: the average altimeter return waveform is the convolution of the ocean surface specular point pdf and a function which depends on the radar parameters alone and is known a priori. One can therefore recover the specular point pdf by performing a deconvolution of the return altimeter signal. If we assume that geometric optics holds, the functional form of the specular point pdf as a function of the SWH, the ocean surface skewness, and the altimeter tracker error is a simple analytic expression which is known from theory [*Barrick and Lipa*, 1985; *Srokosz*, 1986; *Rodríguez*, 1988]. One can easily estimate these parameters by performing a functional fitting of the deconvolved pdf. In contrast, it is not possible in general to obtain a closed form analytic expression for the mean return power [*Rodríguez*, 1988]. This fact makes the functional fitting of the return waveform a significantly more difficult task than the fitting of the specular point pdf.

The advantages of the deconvolution algorithm have encouraged us to make a deeper study of its properties. In this paper we study by means of a Monte Carlo experiment the optimum way of implementing the deconvolution and determine the accuracy of the parameters which may be estimated from the resulting deconvolved specular point pdf.

In the work of *Lipa and Barrick* [1981], the deconvolution of specular points pdfs was carried out only for waveforms that had been averaged for at least 6 s. This limitation was imposed by the fact that the straightforward least squares deconvolution method (or the equivalent use of Fourier transforms) used by Lipa and Barrick is very sensitive to the fading noise of the return altimeter waveform (see *Parker* [1977] for a review of inverse theory for noisy data). In order to reduce the fading noise to the point where the deconvolution method could be applied, Lipa and Barrick was forced to average their data until an acceptable noise level was obtained.

Is this amount of averaging a fundamental limitation of the deconvolution algorithm? If this were the case, the usefulness of such an algorithm would be severely restricted: an algorithm of this type could never be considered for real-time altimeter tracking and parameter estimation, since such data must perforce be obtained at a rate of tens of waveforms per second. In addition, the dynamic character of the altimeter tracker [*MacArthur*, 1978] would restrict the use of an algorithm which acts on waveforms averaged over a long time period to the cases where the tracker noise and transient response could be neglected.

Fortunately, we have a priori knowledge about the shape of the specular point pdf which may be used to reduce the effects of noise on the deconvolution process. Experimentally, we know that the ocean surface pdf is a smooth function which closely resembles a Gaussian pdf [*Phillips*, 1977]. Requiring that the specular point pdf be "smooth" is equivalent to constraining the value of the second derivative of the deconvolved pdf. The fact that the pdf resembles a Gaussian constrains the high-frequency part of the solution's

Copyright 1989 by the American Geophysical Union.

Paper number 89JC00463.
0148-0227/89/89JC-00463$05.00

spectrum to have negligible components in the high-frequency range. Hence one can apply low-pass filtering to the noisy solution to obtain a more accurate estimate of the pdf. Finally, the fact that the deconvolved function is a pdf constrains it to be positive. We have found that, by implementing one or more of these constraints, it is possible to use the deconvolution algorithm on real-time data to obtain estimates of the height error which are biased by only small amounts. In addition, we can use this algorithm to obtain estimates of the significant wave height and ocean surface skewness, which are oceanographic parameters of intrinsic interest.

In order to evaluate the results presented in this paper we mention the accuracy requirements for the TOPEX altimeter [*Jet Propulsion Laboratory*, 1985]. The height accuracy requirement is 2 cm (1σ) for SWH of 2 m. The SWH accuracy requirement is 0.5 m or 10% of SWH, whichever is greater. These requirements are set for three second averages. There is no requirement on the measurement of ocean surface skewness. However, the TOPEX error budget allows for a maximum height error of 1 cm at SWH of 2 m (assuming skewness of 0.1). In this paper, we will be deriving accuracies based on averaging times of 0.1 and 1 s. To obtain the corresponding TOPEX requirements for this averaging time, we multiply the accuracies by $30^{1/2}$ and $3^{1/2}$, respectively, to obtain height accuracy of 11 cm (0.1 s) and 3.5 cm (1 s) for SWH of 2 m; SWH accuracy is 2.7 m or 55% (0.1 s) and 0.85 cm or 17% (1 s), whichever is greater. The TOPEX requirements are the most stringent requirements set on an ocean altimeter yet.

The outline of this paper is as follows: in section 2 we present a brief review of the two convolution models from which the specular point pdf may be obtained starting from the altimeter return waveform. In section 3 we present a brief description of the deconvolution algorithms which we have tested. All of these algorithms already exist in the deconvolution literature, but there are no general criteria which specify which algorithm is most suitable for a given problem. In this section we also describe the fitting algorithm which we have used to estimate the various pdf parameters. In section 4 we describe our simulation model, its assumptions, and its limitations. Section 5 presents the main body of results: we select an optimum algorithm and determine the accuracy of the estimated parameters. In section 6 we examine the effects of having only approximate knowledge of some of the altimeter system parameters on the accuracy of the estimated parameters. Finally, in section 7 we use our algorithms on a set of Seasat waveforms to estimate the various parameters from real data.

2. CONVOLUTION MODELS

In this section we present a very brief review of two convolution models which may be used for the deconvolution of the specular point pdf. A fuller discussion of these convolution models is given by *Lipa and Barrick* [1981], *Barrick and Lipa* [1985], and *Rodríguez* [1988].

In this paper we assume that the specular point pdf is given by [*Barrick and Lipa*, 1985; *Srokosz*, 1986; *Rodríguez*, 1988]

$$f_{sp} = \frac{1}{(2\pi)^{1/2}\sigma} \exp\left(-\eta^2/2\right)\left[1 + \frac{\lambda}{6}(\eta^3 - 3\eta)\right] \qquad (1)$$

$$\eta = \frac{z - z_T}{\sigma} \qquad (2)$$

where σ is the ocean surface standard deviation, λ is the ocean surface skewness, z is the height above the mean ocean surface, and the variable z_T (the tracker bias) represents the shift of the altimeter track point with respect to the mean electromagnetic surface.

In general, the level of the mean electromagnetic surface, which is the surface tracked by the altimeter, will not coincide with the mean of the true ocean surface. This phenomenon is called the electromagnetic (EM) bias [*Barrick and Lipa*, 1985; *Srokosz*, 1986; *Rodríguez*, 1988] and its magnitude is not well determined at present. The total tracker bias (i.e., the shift of the altimeter track point with respect to the true mean ocean surface) is given by the sum of z_T and the EM bias.

It is well known that the mean return altimeter waveform can be expressed as the convolution of the radar point target response (ptr), the "smooth surface response" (SSR) [*Brown*, 1977], and the specular point pdf. Symbolically, we represent this relationship (which we call the "power convolution model") as

$$P(t) = S(t) \otimes \chi(t) \otimes f_{sp}(t) \qquad (3)$$

where $P(t)$ represents the mean return power at time t ($t = 0$ is the time of arrival of the signal from the mean ocean surface); $\chi(t)$ represents the altimeter power ptr, $f_{sp}(t)$ is the specular point pdf in the time domain (obtained by making the change of variables $t = -2z/c$), and $S(t)$ represents the SSR [*Brown*, 1977; *Hayne*, 1980; *Barrick and Lipa*, 1985] and is given by

$$S(t) = A \exp\left(-\alpha t\right) I_0(\beta t^{1/2}) U(t) \qquad (4)$$

where A is a scaling constant, and

$$\alpha = \frac{\ln 4}{\sin^2(\theta/2)} \frac{c}{h} \frac{1}{1 + h/R} \cos(2\xi) \qquad (5)$$

$$\beta = \frac{\ln 4}{\sin^2(\theta/2)} \left[\frac{c}{h} \frac{1}{1 + h/R}\right]^{1/2} \sin(2\xi) \qquad (6)$$

In these equations, c is the speed of light, h is the altimeter height above the mean ocean surface, R is the radius of the Earth, ξ is the altimeter off-nadir pointing angle, θ is the antenna half-power beam width, and $U(t)$ is the unit step function.

A typical mean return altimeter waveform is presented in Figure 1. It can be thought of as consisting of roughly three distinct sections: the first, the "thermal noise only" section, contains the thermal noise power generated by the altimeter prior to the first return of a signal from the ocean surface. The second section, the "leading edge," consists of the return power from the points within the "pulse-limited circle" [*Barrick and Lipa*, 1985]. This section contains all of the useful information about the ocean surface parameters and the altimeter height. The last section, the "trailing edge," consists of the return power from points outside the pulse limited circle. It can be well approximated by a straight line whose slope depends on the altimeter radar beam width and the off-nadir pointing angle.

Equation (3) can be thought of as a matrix equation $y = Mx$, where M is the convolution $S(t) \otimes \chi(t)$, x is the specular

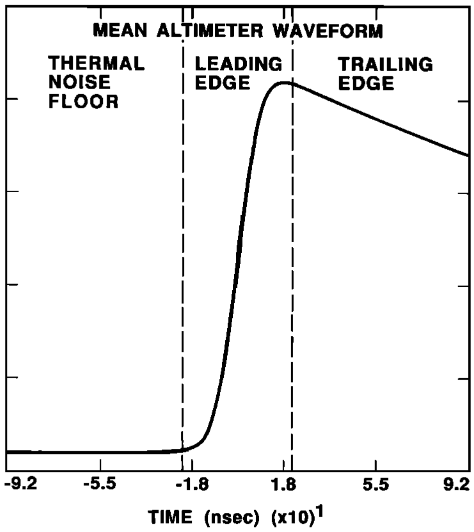

Fig. 1. Typical mean altimeter return waveform from an ocean surface showing the three different sections of which it is composed: the thermal noise floor, leading edge, and trailing edge. The parameters used are those of the TOPEX altimeter.

point pdf, and y is the return power. It is well known that the sensitivity of the numerical solution of a matrix equation is inversely proportional to the conditioning number (the ratio of the largest by the smallest eigenvalue) of the matrix. The conditioning number of (3) can be calculated numerically using typical ocean altimeter parameters and is of the order of 10^9, which implies that in the presence of any noise, (3) is effectively singular.

In order to overcome this problem, *Lipa and Barrick* [1981] introduced a different, but approximate, convolution model. They noticed that when the altimeter antenna gain pattern was neglected, the slope of the return waveform was proportional to the convolution of the specular point pdf and the radar ptr. Since the radar ptr is very narrow in comparison with the width of a typical specular point pdf, its matrix representation is diagonal dominant. Therefore the matrix equation is much better conditioned. Unfortunately, the neglect of the antenna pattern introduces unacceptable biases on the estimated parameters [*Rodríguez*, 1988].

It turns out, however, that the effects of the antenna pattern are easily incorporated when the off-nadir angle is less than a few degrees, which is the situation usually encountered in ocean altimetry. In a separate paper [*Rodríguez*, 1988], we proved that for off-nadir angles less than or of the same order as the antenna beam width, one can express the convolution of the point target response and the specular point pdf as

$$\chi(t) \otimes f_{sp}(t) = \frac{1}{A}\left[P'(t) + \left(\alpha - \frac{\beta^2}{4}\right)P(t)\right] \tag{7}$$

where $P'(t)$ is the derivative of the return power with respect to the return time. We call this model the "corrected slopes convolution model."

From (1), we see that fitting the deconvolved pdf will allow us to estimate three independent parameters: σ, λ, and z_T. In addition, the altimeter return waveform is a function of two other parameters which must be estimated separately: the mean thermal noise and the altimeter off-nadir pointing angle. The effect of the thermal noise is to add a constant power level to the mean waveform. We estimate the magnitude of this constant by averaging the return waveform signal in the "thermal noise only" section of the return waveform. The value of the estimated constant is then subtracted from the return signal to obtain a signal which, in the mean, has no contributions from thermal noise.

The value of the off-nadir pointing angle is usually estimated independently by the satellite. It can also be estimated from the waveform by fitting the slope of the trailing edge. In section 6 we will examine the effects of inexact knowledge of the off-nadir angle on the estimated parameters.

The data from Seasat and Geosat consist of 60 waveform samples, measured at a constant sampling interval of 3.125 ns. Three additional samples were provided in the central part of the leading edge so that the sampling interval in this section is 1.5625 ns. In order to perform the deconvolution, we approximated the integral equations (3) and (7) by the corresponding matrix equations obtained by replacing the integrals by the appropriate trapezoidal quadrature formulas. Furthermore, in order to obtain uniformly sampled data (necessary for taking fast Fourier transforms, or FFTs), we interpolated the data to obtain a uniform 1.5625-ns sampling interval throughout the waveform.

To implement the corrected slopes convolution model, we approximated the derivative by

$$P'(t) = \frac{P(t+\Delta t) - P(t-\Delta t)}{2\Delta t} \tag{8}$$

where Δt is the sampling interval. It was shown by *Rodríguez* [1988] that this approximation of the derivative leads to small biases in the estimated parameters. One may be able to correct for these biases by making the appropriate corrections after the parameters are estimated.

3. DECONVOLUTION AND FITTING ALGORITHMS

For convenience of notation, we will henceforth represent the matrix equation corresponding to either of the convolution models by the equation

$$y = Mx \tag{9}$$

The simplest algorithm which can be used to invert (9) is the least squares algorithm:

$$x = [M^T M]^{-1} M^T y \tag{10}$$

where the superscript T denotes matrix transpose. We implemented this algorithm by using a standard lower triangular–upper triangular (LU) decomposition subroutine to find the matrix inverse. This algorithm does not make use of a priori information about the functional form of the solution. It is also very sensitive to noise. We have found that the results obtained by using this algorithm are nearly identical with the results obtained by applying the FFT based algorithm used by *Lipa and Barrick* [1981]. Hence we will not specifically mention the FFT algorithm in the sections which follow.

A simple way of forcing the deconvolved function to be smooth is to put a constraint on the values which its second derivative may take. A way of implementing this constraint was introduced by *Twomey* [1963], who modified equation (10) to

$$x = [M^T M + \gamma B]^{-1} M^T y \tag{11}$$

where γ is a variable parameter and B is the second derivative operator

$$B = \begin{bmatrix} 1 & -2 & 1 & 0 & 0 & \cdots \\ -2 & 5 & -4 & 1 & 0 & \cdots \\ 1 & -4 & 6 & -4 & 1 & \cdots \\ 0 & 1 & -4 & 6 & -4 & \cdots \\ \vdots & \vdots & \vdots & \vdots & \vdots & \cdots \end{bmatrix} \tag{12}$$

It can be shown that the solution of this equation minimizes the quantity $(Mx - y)^T(Mx - y) + \gamma x^T Bx$. The second derivative of the solution decreases with increasing γ, and therefore "smoother" solutions are obtained. We selected the parameter γ by choosing the largest value of γ which will not significantly bias the parameters estimated from noise-free pdf's. We have implemented the matrix inversion indicated via a LU decomposition matrix inversion routine.

Another constraint which may be applied to the deconvolved specular point pdf is to require that it be nonnegative. *Jansson* [1984] has developed an iterative, nonlinear deconvolution algorithm which forces the solution to be positive. One can write the formula for Gauss-Seidel iterative matrix inversion (or point-simultaneous matrix inversion) as [*Jansson*, 1984]

$$\hat{x}_n^{(j+1)} = \hat{x}_n^{(j)} + \frac{k}{M_{nn}} \left\{ y_n - \sum_m M_{nm} \hat{x}_m^{(j)} \right\} \tag{13}$$

where k is a relaxation constant. To implement the positivity constraint, Jansson modifies this formula by replacing the relaxation constant k by a function of the solution obtained in the previous iterative step. This function is constructed such that it penalizes negative values of x. A standard relaxation function is [*Jansson*, 1984]

$$k[\hat{x}_n^{(j)}] = k_o[\hat{x}_n^{(j)}(1 - \hat{x}_n^{(j)})] \tag{14}$$

where k_0 is a constant which can be changed as the iteration progresses.

A simple way of reducing the high frequency noise of the solution is to Fourier transform the answer obtained from the least squares algorithm, truncate its spectrum at a given cutoff frequency, and transform back to the time domain. We call this method the "low-pass least squares method." The cutoff frequency is selected adaptively based on an approximate determination of σ.

A more sophisticated way of reducing the high-frequency variation of the waveform is the method of singular value decomposition with spectral filtering [*Parker*, 1977]. This method is based on the observation made by *Lanczos* [1961] that the parts of the solution of a matrix equation which are most contaminated by noise are those which lie in the subspaces spanned by the eigenvectors corresponding to the smallest eigenvalues of the matrix operator. Therefore if one projects out the parts of the solution which lie in this subspace, the resulting solution is a much better approximation to the real one (the appendix presents a more mathematical description of this process). In our case, it is true that the eigenvectors corresponding to the smaller eigenvalues of the matrix equation are also the ones which exhibit the greatest oscillatory behavior. Therefore spectral filtering corresponds to low-pass filtering.

We have implemented this algorithm by using a robust singular value decomposition routine given by *Press et al.*

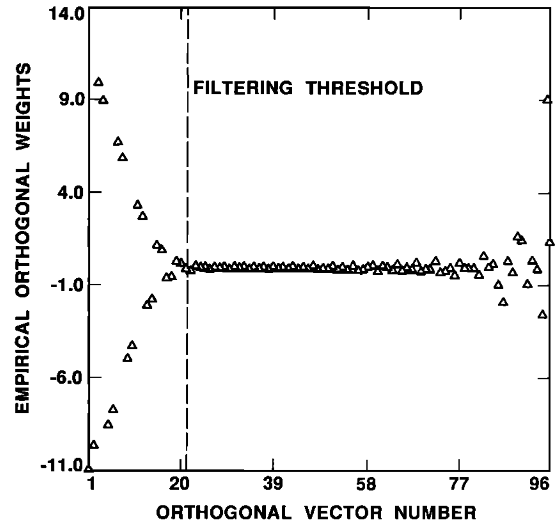

Fig. 2. Values of the empirical orthogonal weights for the singular value decomposition method of deconvolution plotted using the return power for a 4-m SWH noiseless waveform. After a threshold number, the expansion weights are very small and the corresponding vectors may be neglected in the computation of the solution. Notice that for high vector number (which corresponds to high-frequency noise), the weights begin to have nonzero values. This is due to the singular nature of the matrix equation.

[1986]. To select the number of vectors used in the spectral expansion of the solution, we make a preliminary estimate of σ and select the number of vectors necessary to represent a Gaussian with this standard deviation. To see that this number is well determined, examine Figure 2, which represents the weights associated with the spectral expansion for the solution of the power convolution kernel (equation (3)) and $\sigma = 4$ m. As can be seen, the cutoff for the number of vectors which enter in the solution is very well defined. This is typical of all the situations we examined.

A way of introducing the positivity constraint while smoothing the deconvolved pdf was introduced by *Howard* [1984]. The method, called "Fourier continuation," consists of truncating the Fourier transform of the pdf obtained by using equation (11), followed by adaptively selecting new components in the truncated section of the transformed pdf chosen to minimize the negative part of the solution. We obtained the spectral cutoff as well as the number of Fourier coefficients which are to be varied by trial and error. We refer the interested reader to the literature [*Jansson*, 1984] for a fuller account of this algorithm.

Of the algorithms described in the previous paragraphs, only spectral filtering produces an acceptable solution when the power convolution model (equation (3)) is used. The solutions obtained by using the other algorithms are indistinguishable from noise owing to the singular nature of this equation. In contrast, all of the algorithms mentioned produce viable solutions when the corrected slope convolution model (equation (7)) is used.

In order to estimate the specular point pdf parameters, we have linearized equation (1), assuming that $z_T \ll \sigma$, to obtain the fitting function

$$f_{sp} = a \exp(-\zeta^2/2)\left[1 + \frac{\lambda}{6}(\zeta^3 - 3\zeta) + \frac{z_T}{\sigma}\zeta\right] \tag{15}$$

$$\zeta = \frac{z}{\sigma} \tag{16}$$

This linearization is a good approximation given the characteristic behavior of trackers implemented in Seasat, Geosat, and TOPEX. The parameter a in (15) is a scaling parameter introduced to take into account the fact that the deconvolved pdf is not normalized. We have estimated the parameters a, σ, λ, and z_T by using a nonlinear, iterative, least squares fitting algorithm given by *Press et al.* [1986] based on the Levenberg-Marquardt method [*Marquardt*, 1963]. The fitting procedure was performed in two steps: The initial step performed a rough estimation of the parameters. Based on this estimate, the data points outside a 4σ interval about the estimated mean of the pdf were set equal to zero. The parameters were then estimated using this modified data. The reason behind this procedure is that since the waveform noise is multiplicative, the noise on the tail of the pdf which corresponds to the troughs of the waves is much greater than the noise in the rest of the deconvolved pdf. Since we know that the pdf is approximately Gaussian, setting the data to zero outside a 4σ interval is a good approximation and will discard the noisiest parts of the deconvolved pdf. The determination to use a 4σ interval was made by trial and error. It turns out that if σ is known exactly, a smaller value for the size of the interval will give somewhat better results. However, due to uncertainties in the estimation of σ, a value of 4σ proves to be more robust in the presence of noise.

The total running time of these algorithms varies according to which algorithm is chosen. However, for the "optimum" algorithms chosen in the next section, the total running time (including deconvolution and parameter estimation) was less than 1 s per waveform in a micro-VAXII computer. Since we have not optimized the algorithms with respect to running time, we expect that an optimum implementation which operates in real time is possible. A possible way of accomplishing this is to implement a tracking filter for the various parameters to be estimated. The previous estimated value of the parameters can be used as a first approximation to the real value. One can then fully linearize the fitting function about these values. In this case, the parameter estimation reduces to a simple 3 × 3 matrix inversion. Furthermore, the previous value of the SWH may be used in order to truncate the pdf, as was mentioned in the preceding paragraph.

4. MONTE CARLO SIMULATION

In order to determine the accuracies with which the various parameters may be estimated from deconvolved pdf's, we have set up a Monte Carlo simulation of the deconvolution and estimation process. The simulation is divided into three main parts: (1) noisy waveform generation, (2) deconvolution, and (3) estimation of parameters. The last two parts were described in the preceding section. This section presents a description of the generation of simulated noisy altimeter waveform data.

In order to generate a noisy return waveform, we numerically perform the convolution of the radar ptr, the surface impulse response, and the specular point pdf by means of FFTs. The parameters characterizing each of these functions can be varied at will, and we can use either a theoretical $\sin^2(\pi Bt)/(\pi Bt)^2$ ptr [*Ulaby et al.*, 1982] (B is the altimeter pulse bandwidth), or the ptr's obtained from the calibration of the Seasat [*Barrick et al.*, 1980] and Geosat [*Applied Physics Laboratory*, 1985] altimeters.

After selecting the number of waveforms to be averaged together, we superimpose Gaussian random noise on each mean waveform sample. The Gaussian noise superimposed on the power received at time t has a standard deviation given by

$$\sigma_P = \frac{P(t)}{[N_{\text{ind}}(t)]^{1/2}} \tag{17}$$

where $P(t)$ is the mean return power at time t and $N_{\text{ind}}(t)$ is the number of independent samples at time t. A typical altimeter waveform consists of the average of many (typically, at least 50) individual returns. Therefore although the noise in each return is exponentially distributed, the central limit theorem implies that it is a good approximation to assume that the averaged return noise is Gaussian.

It is important to notice that owing to the effects of the pulse-to-pulse correlation of the returned field, the number of independent samples need not be equal to the number of averaged waveforms (see *Berger* [1972] for a fuller discussion of this point). This effect is most noticeable in the leading edge of the waveform, where there are in general fewer independent samples than in the rest of the waveform (see *Lipa and Barrick* [1981] for an empirical confirmation of this effect for the Seasat altimeter). This is unfortunate, since it is precisely the leading edge of the waveform that contains the information about the ocean surface parameters. Not including these pulse-to-pulse correlation effects in the simulation would result in overly optimistic predictions about the accuracy with which parameters can be recovered.

The number of independent samples can be calculated once the correlation time for a given waveform sample is known by means of the formula

$$N_{\text{ind}} = \frac{f_a T_{\text{ave}}}{T_{\text{corr}}} \tag{18}$$

where f_a represents the pulse repetition frequency (PRF) of the altimeter, T_{ave} is the averaging time, and T_{corr} is the correlation time for the waveform sample. T_{corr} is related to the correlation distance r_c by the relation $T_{\text{corr}} = r_c/v_s$, where v_s is the spacecraft velocity. We can then write the relation

$$N_{\text{ind}} = \frac{f_a v_s T_{\text{ave}}}{r_c} \tag{19}$$

The correlation length can be calculated by modifying the equations derived by *Berger* [1972] for a Gaussian ptr and a flat Earth to include a realistic ptr and a curved Earth. We have developed these formulas; however, we have found that for our purposes it is adequate to use the van Cittert-Zernike (vCZ) theorem [*Born and Wolf*, 1980; *Walsh*, 1982] to calculate this correlation length. The vCZ theorem states that the correlation coefficient of the electric field is proportional to the Fourier transform of the illumination. (We note that the derivation presented by *Born and Wolf* [1980] assumes one-way propagation of radiation. The generalization to round-trip propagation must be made in order to apply the theorem to radars. The alteration of the theorem is trivial, however, and merely introduces an overall multiplicative factor of 2 in the phase of the transform.)

It is easy to show that for a nadir-pointing altimeter with a pulse of bandwidth B, the illuminated area is well approxi-

TABLE 1. Altimeter Parameters

Altimeter	Height, km	Beam Width, deg	Bandwidth, MHz	Sampling Time, ns	PRF, Hz
Seasat	800	1.6	320	3.125	1020
Geosat	800	2.1	320	3.125	1020
TOPEX	1334	1.0	320	3.125	4000

mated by (1) a circle of radius $\rho = [hc(t + \tau/2)/(1 + h/R)]^{1/2}$ for $-\tau/2 \le t \le \tau/2$ (the leading edge of the waveform) and by (2) an annulus of outer radius $\rho = \{hc(t + \tau/2]/(1 + h/R)\}^{1/2}$ for $t \ge \tau/2$ (the trailing edge). The "effective pulse length" τ is given by

$$\tau = \left[\left(\frac{1}{B}\right)^2 + \left(\frac{4\sigma}{c}\right)^2\right]^{1/2} \tag{20}$$

The formula for the correlation coefficient of the electromagnetic field for these illuminated areas is well known [*Born and Wolf*, 1980] (assuming that the illumination can be regarded as constant over the illuminated area). Defining the first zero crossing of this function as the correlation length, one can compute the correlation length for the circle or the annulus numerically. We have computed these zero crossings numerically and programmed them as look-up functions in the noise generation part of our simulation.

Altimeter returns can also exhibit correlation between different time bins [*Lipa and Barrick*, 1981]. In the present simulation, we have neglected bin-to-bin correlation mainly because we have found that implementing it would cause an unacceptable increase in our computation time. This neglect is justified for the theoretical ptr, since in this case, the bin-to-bin correlation is small. However, ptr's which exhibit greater side lobes may have larger bin-to-bin correlation. We defer consideration of this effect for later work.

In order to simulate the effects of altimeter tracker jitter, we have implemented a simple "$\alpha - \beta$" filter [*Benedict and Bordner*, 1962] (the constants α_t and β_t introduced here should not be confused with the constants introduced in equation (4)). The equations for this filter are given by

$$\bar{x}_n = x_{pn} + \alpha_t(x_n - x_{pn}) \tag{21}$$

$$\bar{v}_n = \bar{v}_{n-1} + \frac{\beta_t}{T}(x_n - x_{pn}) \tag{22}$$

$$x_{pn} = \bar{x}_{n-1} + Tv_{n-1} \tag{23}$$

where x_n represents the (noisy) height measurement made by the altimeter; $\bar{x}_n$ represents the estimated height at the nth iteration; $\bar{v}_n$ represents the estimated velocity at the nth iteration; x_{pn} represents the predicted height; and T is the filter update time. To simulate the behavior of the altimeter tracker, we generated random, zero mean, Gaussian values of arbitrary standard deviation for x_n and used the tracker equation to estimate $\bar{x}_n$. We then applied a shift equal to $\bar{x}_n$ to the simulated waveform. This procedure should provide a good simulation of steady state altimeter tracking. It is not adequate to simulate transient tracking behavior, since in this case the altimeter must make velocity corrections to the individual waveforms [*MacArthur*, 1978] and the details of the timing and implementation of the tracker become crucial to predicting the tracker behavior. In our simulation we have used the values $\alpha_t = 1/4$, $\beta_t = 1/64$, and $T = 0.05$ s. These values correspond to the ones used for nominal tracking mode in the Seasat altimeter.

In order to compare the behavior of our algorithms against the look-up table type algorithms implemented in the Seasat and Geosat altimeters, we have followed *MacArthur*'s [1978] construction of the look-up tables. The main difference between our look-up algorithms and the ones described by MacArthur is that we have included both the slope and intercept of the height look-up linear templates (Seasat used only the slopes). This eliminates the sea state bias mentioned by *Hayne and Hancock* [1982], *Born et al.* [1982], *Douglas and Agreen* [1983], and *Barrick and Lipa* [1985]. In addition, we have assumed that the SWH is known exactly, so the correct look-up template is always consulted. These modifications should improve the performance of the simulated tracker over that of the Seasat tracker.

Another instrument effect which was incorporated into our simulation is the fact that the gains for the waveform sample filters may vary from sample to sample [*Townsend*, 1980; *Hayne*, 1980]. These gains may be determined with finite accuracy from calibration data. We model the error in determining the gain of each filter as Gaussian multiplicative noise. The standard deviation of the noise depends on the accuracy with which the gains may be calibrated.

For any given set of parameters, we used 1000 noisy waveform realizations in the Monte Carlo simulation to determine the parameter estimation accuracy. We estimated the number of realizations needed in order to reduce the sampling error by varying the number of realizations used and calculating the variance of the estimates for each number of realizations. We then extrapolated the $1/N^{1/2}$ behavior of this variance until it met our accuracy requirement. The actual number of realizations chosen (1000) is a conservative overestimate of this number.

5. Simulation Results

In order to select an optimum deconvolution algorithm, we have devised a two-step selection procedure. The first step is independent of the fitting algorithm and of the specific functional form of the pdf used, while the second step uses the least squares fitting algorithm to estimate the biases and noise peculiar to the algorithms.

The test data used to evaluate the algorithms were generated by using the TOPEX altimeter parameters (see Table 1). The ocean surface parameters used were SWH = 2, 4, 8 m and $\lambda = 0.0, 0.3$. This Monte Carlo simulation consisted of deconvolving 1000 simulated noisy realizations, each waveform corresponding to a 0.1-s averaging time. The results of the evaluation are presented in Table 2.

We have selected four criteria to evaluate the deconvolution algorithm independently of the fitting method and functional form of the pdf. The first criterion is the root sum square (rss) difference between the deconvolved pdf and the true pdf. In order to make comparisons easier, we first

TABLE 2. Evaluation of Algorithms

Algorithm	rss	Mean Height	Variance	Complexity	Robustness	Skewness* Mean	Skewness* rms	Height Error* Mean	Height Error* rms	SWH* Mean	SWH* rms
Power deconvolution											
SVDSF	1.20	1.00	1.37	low	high	2.13	1.57	1.00	1.55	1.91	1.22
Corrected Slope Deconvolution											
SVDSF	1.14	1.17	1.40	low	high	1.00	1.55	1.74	1.55	1.00	1.27
LU Decomposition	5.53	3.42	10.69	low	moderate	4.15	2.21	2.03	1.65	1.83	1.77
LPLS	1.00	1.95	1.00	moderate	moderate	2.90	1.00	1.43	1.23	2.12	1.00
Fourier Continuation	0.77	0.60	0.06	high	low	6.16	0.09	2.13	0.77	18.63	0.50
Twomey	2.90	2.09	4.18	low	high	3.05	1.07	2.02	1.00	1.27	1.05
Jansson	3.00	38.82	28.17	high	low	7.12†	1.25†	10.09†	1.69†	1.55†	1.37†

SVDSF, singular value decomposition with spectral filtering; LPLS, low-pass least squares.
*Fitted parameters.
†SWH = 2, 4 m.

normalized the rss with the minimum value of the rss difference at each sea state. This number is then relatively independent of sea state. We then found the average normalized rss for each algorithm averaged over the six possible sea states. The final comparison is made by normalizing by the minimum value, which is associated with the best performing algorithm (Fourier continuation was excluded owing to its eccentric behavior). This procedure enabled us to obtain a clear ranking of each algorithm.

The second criterion involves the determination of the mean surface height bias and variance, where the mean height is calculated by means of the formula

$$\langle z \rangle = \frac{\sum_i z_i \hat{f}_i}{\sum_i \hat{f}_i} \tag{24}$$

where $\hat{f}_i$ is the ith sample of the deconvolved pdf, and z_i is the corresponding surface height. This procedure for calculating the mean surface height is independent of the functional form assumed for the pdf. We calculated the mean height bias and its variance, and normalized by sea state and algorithm, as we did with the rss (Fourier continuation was again excluded).

The third performance criterion is the "complexity" of the algorithm. We judged that an algorithm had "low" complexity if it could be implemented by using a set of matrix inverses (which may depend on SWH and altimeter pointing) which may be stored in look-up tables. An algorithm which needs, in addition to stored matrix inverses, to take FFTs in order to perform low-pass filtering we judged to be "moderately complex." Finally, an algorithm which has to be implemented iteratively we judged as having a "high" complexity. There is a relation between the complexity (as defined here) of an algorithm and the amount of CPU time it uses to perform a deconvolution.

The fourth performance criterion is the "robustness" of the algorithm. We called an algorithm of "high" robustness if it never encountered a singular matrix or failed to converge while deconvolving data corresponding to the shortest averaging time (and, therefore, greatest noise) used in the simulation. An algorithm was "moderately robust" if it seldom failed to converge or encountered a singular matrix. Conversely, an algorithm was of "low" robustness if it regularly encountered singular matrices or failed to converge during the deconvolution process.

The second step of the selection procedure is the comparison of the estimated parameters obtained by least squares fitting (see section 3) of the deconvolved pdf's. We tabulated the mean skewness, height error, and SWH for each algorithm and sea state and then calculated the normalized value with respect to sea state and algorithm, as we did for the comparison of the rss, and the mean height and its variance. (Fourier continuation was again excluded on account of its eccentric behavior).

As can be seen from Table 2, the low-pass least squares (LPLS) method yields the smallest comparative rss and variance, though singular value decomposition with spectral filtering (SVDSF) of the power and the corrected slope is comparable. The smallest comparative bias in the mean height is found by SVDSF of the power. LU decomposition and Jansson's method perform the most poorly in estimating the mean value of the parameters, while Twomey's algorithm occupies a middle ground. Fourier continuation apparently performed very well in the rss, mean height, and the variance, but only because the form of the pdf was excessively smoothed and distorted by the algorithm. This is evident from examining the results of the mean of the fitted parameters. This is the reason this algorithm was excluded in the comparison of the algorithms, though the results are included for reference.

In the estimation of the skewness, SVDSF of the corrected slope was the least biased, while LPLS had the smallest comparative rms. In the estimation of the mean height error, SVDSF of the power was the least biased, while Twomey's method had the smallest comparative rms. In the estimation of the SWH, SVDSF of the corrected slope was the least biased, and LPLS had the smallest comparative rms. The values for Jansson's method are only for SWH of 2 and 4 m, as Jansson's method was not robust enough to obtain meaningful statistics at a SWH of 8 m. Fourier continuation was the most biased for all three parameters.

Because of their small biases and variances, robustness, and ease of implementation, we selected the singular value decomposition algorithms as the two optimum ones in the set we studied. The rest of this section presents a more detailed characterization of these two algorithms.

To test a representative set of altimeters, we used the parameters corresponding to the Seasat and TOPEX altimeters (see Table 1). To assess the ability of the algorithms to

TABLE 3a. Height Statistics for 0.1-s Time Average Using TOPEX Parameters (Power Algorithm)

SWH, m	Skewness 0.0 Bias	0.0 s.d.	0.15 Bias	0.15 s.d.	0.30 Bias	0.30 s.d.	0.45 Bias	0.45 s.d.
1	0.6	7.7	0.4	7.7	0.1	7.8	0.1	7.8
2	0.4	10.5	0.2	10.2	0.0	10.0	−0.2	9.8
3	−0.1	13.1	−0.2	12.7	−0.4	12.4	−0.6	12.2
4	0.2	14.4	0.0	13.9	0.0	13.4	−0.1	12.9
5	0.5	16.7	0.4	16.0	0.3	15.4	0.2	14.8
6	0.4	15.9	0.2	15.2	0.1	14.4	0.1	13.8
7	0.5	16.9	0.3	16.2	0.1	15.5	0.0	14.9
8	0.1	18.6	−0.2	17.8	−0.2	17.0	−0.2	16.2
9	0.6	18.3	0.5	17.4	0.4	16.5	0.3	15.7
10	0.0	19.7	−0.1	18.8	−0.1	17.9	−0.1	17.0

Values are in centimeters.

TABLE 3c. Skewness Statistics for 0.1-s Time Average Using TOPEX Parameters (Power Algorithm)

SWH, m	Skewness 0.0 Bias	0.0 s.d.	0.15 Bias	0.15 s.d.	0.30 Bias	0.30 s.d.	0.45 Bias	0.45 s.d.
1	0.16	1.1	0.05	1.1	−0.06	1.1	0.17	1.0
2	0.07	1.0	0.02	0.9	−0.03	0.9	0.09	0.9
3	0.06	0.9	0.03	0.9	0.00	0.8	−0.03	0.8
4	0.07	0.7	0.06	0.7	0.05	0.7	0.03	0.7
5	0.08	0.7	0.07	0.6	0.06	0.6	0.05	0.6
6	0.06	0.5	0.05	0.5	0.04	0.5	0.03	0.4
7	0.05	0.4	0.04	0.4	0.03	0.4	0.03	0.4
8	0.03	0.4	0.03	0.4	0.02	0.4	0.02	0.4
9	0.04	0.4	0.04	0.4	0.03	0.3	0.03	0.3
10	0.03	0.4	0.02	0.4	0.02	0.04	0.02	0.3

perform on telemetry data, we used simulated data corresponding to an averaging time of 0.1 s (the data rate of the Seasat and Geosat altimeters). As an example, the results for the TOPEX altimeter using the power algorithm are presented in Table 3. A similar set of results for the slope algorithm is presented in Table 4. A comparison of the height error estimation performance between the deconvolution algorithms and the look-up table algorithm is presented in Figure 3.

From these results, the following conclusions may be drawn:

1. The power algorithm suffers from very small biases in the estimated height. By contrast, the corrected slopes algorithm suffers from centimeter level biases for all values of SWH. These biases are due to the approximate way the waveform slope was calculated.

2. The biases due to changing skewness are negligible (millimetric) for the deconvolution algorithms. The skewness biases incurred by the look-up are much greater than those incurred by either of the two deconvolution algorithms.

3. The height noise of both deconvolution algorithms is about 2 times larger than that of our idealized look-up table algorithm for all values of SWH. Nevertheless, the deconvolution algorithms still meet the noise performance requirement of the TOPEX mission.

TABLE 3b. SWH Statistics for 0.1-s Time Average Using TOPEX Parameters (Power Algorithm)

SWH, m	Skewness 0.0 Bias	0.0 s.d.	0.15 Bias	0.15 s.d.	0.30 Bias	0.30 s.d.	0.45 Bias	0.45 s.d.
1	25	24	25	24	25	24	25	24
2	8	33	8	33	9	33	9	34
3	3	44	3	44	3	45	4	45
4	−6	49	−5	50	−3	51	−2	52
5	−5	58	−4	60	−3	61	−1	62
6	0	58	0	59	1	60	2	61
7	−1	61	0	62	0	63	1	64
8	−6	64	−5	65	−3	66	−2	66
9	−4	68	−3	70	−2	71	−2	72
10	−5	67	−4	68	−3	69	−1	70

Values are in centimeters.

4. Both deconvolution algorithms have small biases in the estimation of SWH. The bias may be corrected with good accuracy, since it is not very dependent on SWH or skewness.

5. Even for 0.1-s data, the SWH noise meets the Geosat and TOPEX performance requirements (10% of SWH or 50 cm, whichever is greater). This requirement is set for 3-s averages.

6. The bias of the estimated skewness for SWH greater than 1 m is small (less than 0.1). The bias is greater for 1-m SWH. However, for low values of SWH, the skewness has a negligible effect on the altimeter measurement, and its effect need not be corrected.

7. The rms noise on the skewness decreases with SWH. The skewness estimated from 0.1-s data is too noisy to make a useful determination of the skewness. Therefore if better estimates of the skewness are desired, skewness estimates must be averaged. The longer averaging time is also desirable because the biases on the estimated skewness decrease with longer averaging time.

8. The TOPEX altimeter performed significantly better than the Seasat altimeter in the estimation of all the parameters. This is due to the effects of higher PRF. Although the number of independent samples in the beginning to middle sections of the leading edge is not that much greater for TOPEX (owing to pulse-to-pulse correlation), the later part of the leading edge, the trailing edge and the noise-only sections have 4 times as many independent samples.

9. Since the height noise performance of both algorithms is comparable, but the algorithm which uses the return power is less biased than the one which uses the corrected slopes, we have selected the SVDSF power algorithm as the optimum algorithm from the set of algorithms studied. In the

TABLE 4a. Height Statistics for 0.1-s Time Average Using TOPEX Parameters (Slope Algorithm)

SWH, m	Skewness 0.0 Bias	0.0 s.d.	0.15 Bias	0.15 s.d.	0.30 Bias	0.30 s.d.	0.45 Bias	0.45 s.d.
2	3.6	10.9	3.5	10.6	3.4	10.3	3.2	10.1
4	3.1	14.5	2.9	14.0	2.7	13.5	2.6	12.9
8	2.9	17.6	2.7	16.8	2.5	16.1	2.3	15.4

Values are in centimeters.

TABLE 4*b*. SWH Statistics for 0.1-s Time Average Using TOPEX Parameters (Slope Algorithm)

SWH, m	Skewness 0.0 Bias	0.0 s.d.	0.15 Bias	0.15 s.d.	0.30 Bias	0.30 s.d.	0.45 Bias	0.45 s.d.
2	0	34	−1	34	−2	34	−2	35
4	−7	48	−7	49	−6	50	−6	50
8	−5	64	−5	65	−5	66	−5	66

Values are in centimeters.

rest of this paper, we will concentrate only on the properties of this algorithm.

To study the behavior of the parameter estimation as a function of the averaging time, we simulated data with averaging times of 0.05, 0.1, 0.4, 1.6, and 6.4 s. The maximum distance traveled by the altimeter during this period is approximately 40 km. This is not a large distance compared with the scales over which ocean surface parameters are believed to change. (As a reference, for later comparison with the Seasat data, we present the characteristics of the simulated Seasat altimeter for 1-s averaging time in Table 5.) We found that when more than 100 waveforms are averaged together, the random noise in the estimated parameters decreases as $T_{\mathrm{ave}}^{-1/2}$, where T_{ave} is the averaging time. However, if fewer than approximately 400 waveforms are averaged, the skewness estimate can be biased high significantly. The height and SWH estimates are not similarly affected. This bias disappears for larger averaging times. Since λ is not expected to change in the scale of a few kilometers, it may be advantageous to estimate it from pdf's averaged over a longer time period.

On the other hand, we have found that when the number of waveforms averaged was small (50 for TOPEX, 100 for Seasat), the algorithm did not perform as well as the $T^{-1/2}$ behavior would predict. This may be due to the fact that the correlation between the height bias and the skewness is large (about −0.7). When the number of averaged waveforms is small, the tail of the pdf tends to be very noisy, and the estimated skewness is very biased. This significantly contaminates the height estimate. A corollary of this observation is that if the skewness is not estimated, the random noise of the height estimate should be significantly lower than when both parameters are estimated. That this in fact happens is shown in Figure 4, where we present a comparison of the standard deviation and bias of the height noise of 0.1-s-averaged waveforms when λ is and is not estimated for varying SWH. The parameters used are those of the TOPEX altimeter.

TABLE 4*c*. Skewness Statistics for 0.1-s Time Average Using TOPEX Parameters (Slope Algorithm)

SWH, m	Skewness 0.0 Bias	0.0 s.d.	0.15 Bias	0.15 s.d.	0.30 Bias	0.30 s.d.	0.45 Bias	0.45 s.d
2	0.15	1.1	0.11	1.1	0.08	1.1	0.04	1.1
4	0.08	0.8	0.07	0.7	0.05	0.7	0.04	0.7
8	0.03	0.4	0.02	0.4	0.01	0.4	0.01	0.4

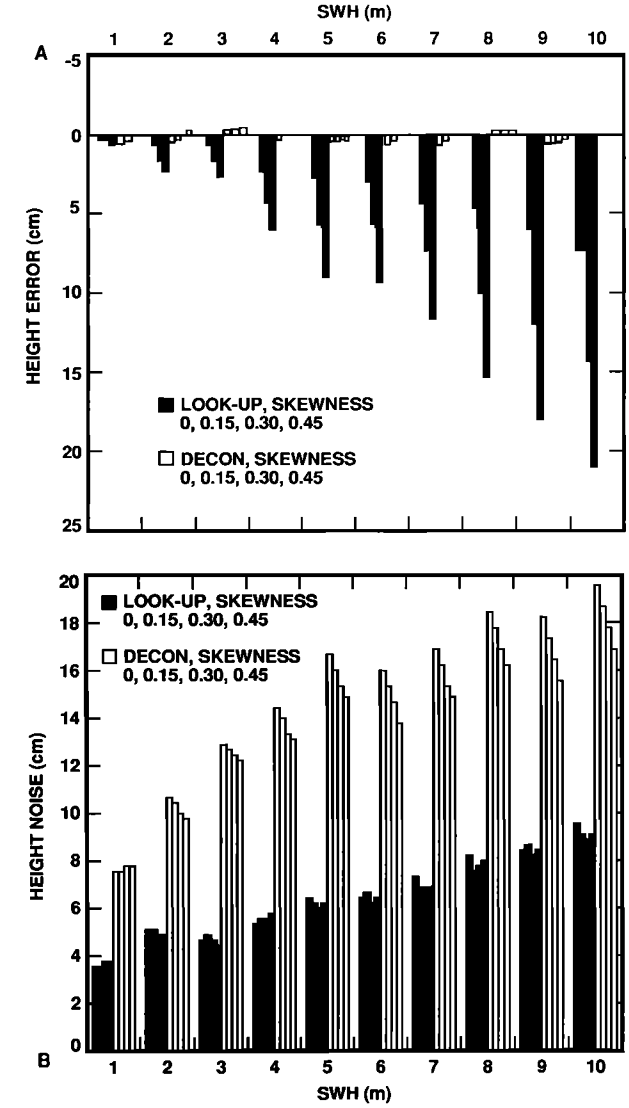

Fig. 3. (*a*) Comparison of the height biases of the deconvolution algorithm with those of the look-up table for varying SWH and skewness. (*b*) Standard deviations of the estimated height for these two estimation algorithms.

In order to show that the estimation of parameters from averaged pdf's is a viable alternative, at least in the case where steady state tracking applies, we simulated sequences of 0.05-s waveforms for SWH = 2,4 m which suffered from tracker jitter. We then averaged the results over various averaging times and estimated the parameters. The description of the tracker jitter implementation was presented in the last section. The standard deviation picked for the estimated height error was 10 cm for 2-m SWH and 20 cm for 4-m SWH. The numbers chosen are noisier than our estimates of the tracking jitter noise obtained by our simulation of the look-up table algorithm in order to obtain a conservative estimate of this effect. The results of this simulation showed no noticeable change in the biases or variances from those obtained when the tracker jitter was neglected. This result implies that at least for situations where the tracker dynamics can be neglected and where the tracker jitter is of reasonable magnitude, one can improve the results of the deconvolution algorithm by averaging the deconvolved pdf's. The averaging time is then governed by the length scale of the oceanographic signal one is trying to observe.

TABLE 5a. Height Statistics for 1-s Time Average Using Seasat Parameters (Power Algorithm)

SWH, m	Skewness 0.0 Bias	s.d.	0.15 Bias	s.d.	0.30 Bias	s.d.	0.45 Bias	s.d.
1	1.1	4.1	0.8	4.1	0.6	4.0	0.4	4.0
2	0.6	6.0	0.3	5.8	0.1	5.6	0.2	5.5
3	0.1	8.0	0.5	7.7	0.2	7.4	0.3	7.1
4	0.2	10.2	0.1	9.8	0.1	9.3	0.1	8.9
5	0.3	10.7	0.3	10.2	0.3	9.7	0.3	9.1
6	0.4	10.7	0.2	10.1	0.1	9.6	0.0	9.1
7	0.5	11.2	0.3	10.6	0.2	10.1	0.0	9.6
8	0.4	13.0	0.3	12.3	0.3	11.7	0.2	11.0
9	0.4	12.3	0.3	11.7	0.2	11.0	0.1	10.4
10	0.1	13.8	0.0	13.1	−0.1	12.4	−0.1	11.7

Values are in centimeters.

TABLE 5c. Skewness Statistics for 1-s Time Average Using Seasat Parameters (Power Algorithm)

SWH, m	Skewness 0.0 Bias	s.d.	0.15 Bias	s.d.	0.30 Bias	s.d.	0.45 Bias	s.d.
1	0.18	0.6	0.07	0.6	−0.04	0.6	−0.15	0.6
2	0.05	0.5	0.0	0.5	−0.05	0.5	−0.10	0.5
3	0.03	0.5	0.0	0.5	−0.01	0.5	−0.03	0.5
4	0.04	0.5	0.03	0.5	0.02	0.4	0.01	0.4
5	0.04	0.4	0.04	0.4	0.03	0.4	0.03	0.4
6	0.03	0.3	0.02	0.3	0.02	0.3	0.01	0.3
7	0.03	0.3	0.02	0.3	0.02	0.3	0.01	0.3
8	0.03	0.3	0.02	0.3	0.02	0.3	0.02	0.3
9	0.02	0.2	0.02	0.2	0.02	0.2	0.01	0.2
10	0.02	0.3	0.01	0.2	0.01	0.2	0.01	0.2

6. Attitude and Calibration Errors

In order to perform the deconvolution of the specular point pdf, one must have knowledge of the altimeter pointing angle. This angle can be obtained either from the satellite sensors or from the return waveform [*Barrick and Lipa*, 1985; *Wingham*, 1988]. Either way, the estimated attitude will be noisy. In order to test the sensitivity of our algorithm to an error in the estimated attitude, we generated noiseless waveforms with a given attitude and performed the deconvolution assuming a varying attitude error. The parameters used were those of the TOPEX altimeter, since its narrow beam width makes it the most sensitive to attitude errors. The resulting errors in the height and skewness are presented in Figure 5 for the case of a nadir-pointing altimeter and attitude estimation errors ranging from 0° to 0.3°. We do not plot the SWH error because it is very small. As a comparison, we present in Figure 5*a* the height errors induced by mispointing on the look-up table algorithm.

Examination of Figures 5*a* and 5*b* shows that the deconvolution algorithm produces results which are only slightly biased if the attitude is known to an accuracy of approximately 0.2°. One should contrast this result with the height errors induced on the look-up table algorithm (Figure 5): the look-up algorithm is obviously much more sensitive to an error in attitude estimation. The pointing accuracy for the TOPEX altimeter will be 0.07° (1σ), which will be more than adequate as an input to the deconvolution algorithm.

TABLE 5b. SWH Statistics for 1-s Time Average Using Seasat Parameters (Power Algorithm)

SWH, m	Skewness 0.0 Bias	s.d.	0.15 Bias	s.d.	0.30 Bias	s.d.	0.45 Bias	s.d.
1	24	14	25	14	25	14	25	14
2	9	19	10	20	10	20	10	20
3	5	25	5	25	6	26	6	26
4	2	29	2	30	3	31	3	32
5	1	33	1	35	2	36	2	37
6	2	35	2	36	3	37	3	38
7	2	37	2	38	2	39	3	40
8	1	38	−1	40	0	41	1	42
9	0	41	0	43	0	44	1	45
10	1	42	−1	43	0	45	1	47

Values are in centimeters.

A second source of error is the lack of exact calibration of the gains associated with each waveform sample. In order to study the influence of this error source on the estimated parameters, we simulated the error in calibration as multi-

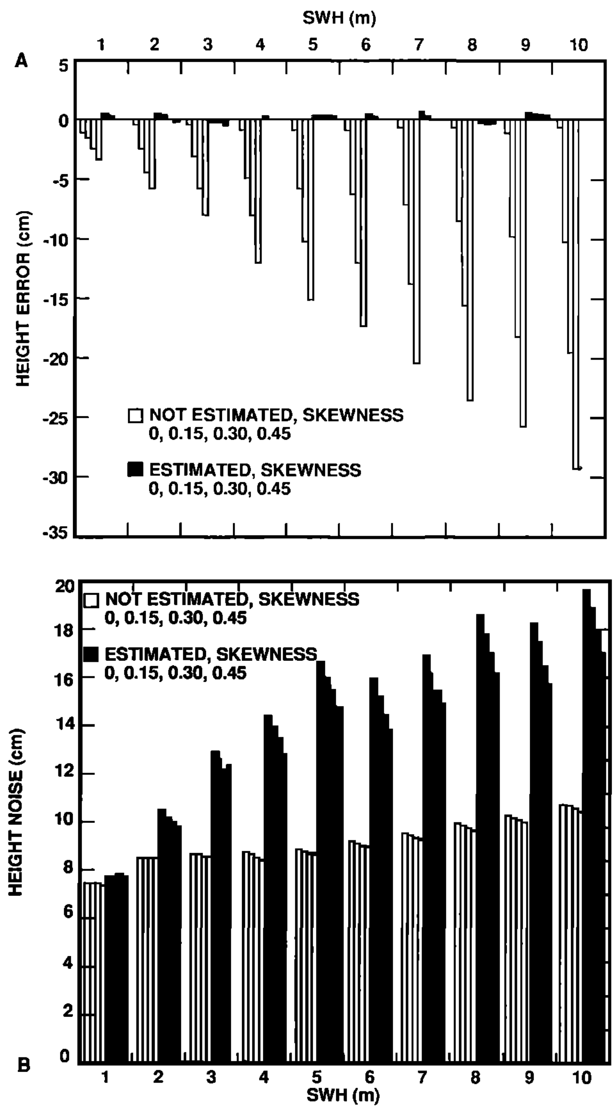

Fig. 4. (*a*) Comparison of the height biases of the deconvolution algorithm when skewness is and is not estimated. (*b*) Standard deviations of the estimated height for the same case.

plicative Gaussian noise whose variance depends on the calibration accuracy. The resulting biases for the estimated parameters as a function of the calibration accuracy for SWH of 2 m, 4 m, and 8 m are presented in Figure 6.

It is evident from Figure 6 that in order to perform the accurate estimation of the parameters, the filter gains must be known to great accuracy. In particular, the estimation of the ocean surface skewness is extremely sensitive to errors in filter gain calibration. We estimate that in order for this parameter to be estimated successfully, one must know the filter gains with a precision of at least 1% (or, preferably, 0.5%) of their true value.

The altimeter height is also sensitive to calibration errors. To achieve a height bias of less than 2 cm for 2-m SWH, one must know the gains to an accuracy of 1%. To compare the sensitivity to calibration error of the deconvolution algorithm height estimation to the sensitivity of the look-up table algorithm height estimation, we estimated the height biases incurred by this last algorithm using the same set of simulated data. The results are shown in Figure 7. One can see that the look-up table algorithm is about half as sensitive to calibration gain uncertainties as the deconvolution algorithm.

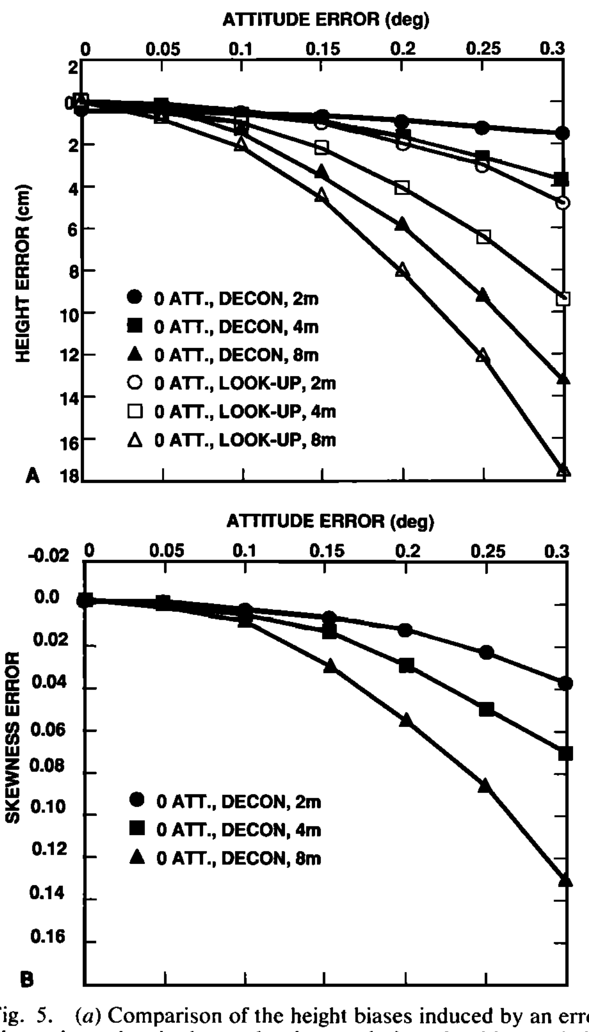

Fig. 5. (*a*) Comparison of the height biases induced by an error in the estimated attitude on the deconvolution algorithm and the look-up table algorithm for 2-m, 4-m, and 8-m SWH. Notice that for smaller SWH, the deconvolution algorithm is significantly less biased. (*b*) Biases induced in the estimated skewness for the same values of SWH and estimated mispointing.

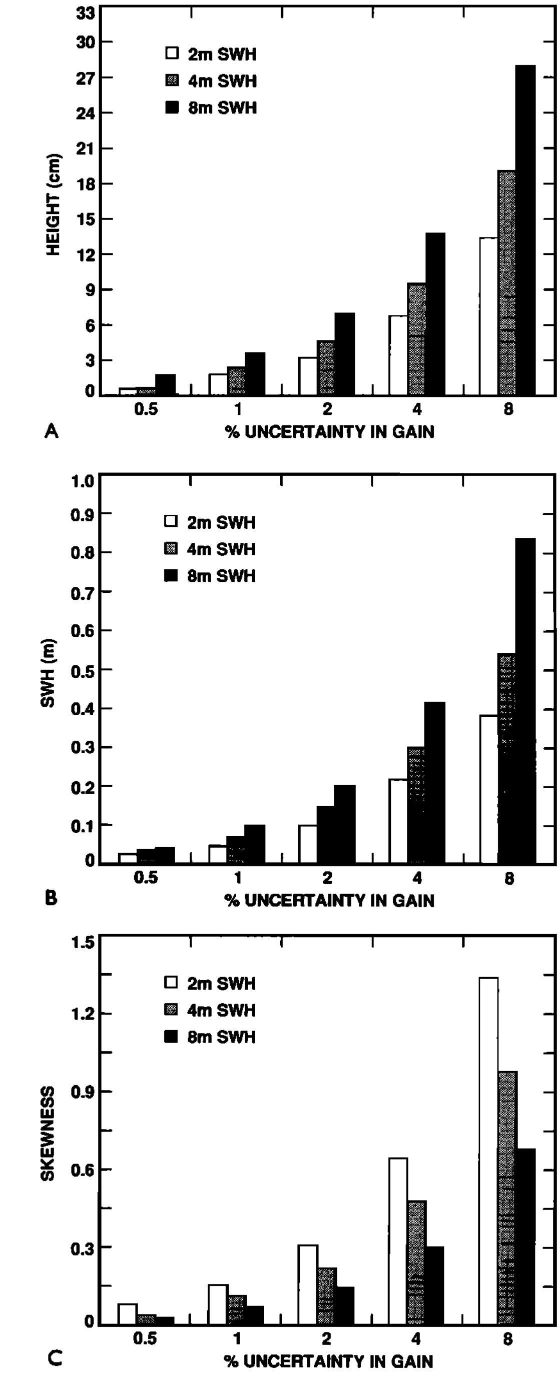

Fig. 6. Biases in (*a*) height, (*b*) SWH, and (*c*) skewness (1σ) for the deconvolution algorithm due to random errors in the altimeter filter gain calibration for various values of calibration accuracy.

The altimeter point target response is determined through calibration. There are two main sources of error in using this ptr in the deconvolution algorithm: (1) the calibration has finite accuracy and (2) we need to interpolate the ptr from the calibration points: this introduces interpolation errors. In order to simulate these error sources, we used a ptr of the form

$$\chi(t) = \frac{\sin^2(\pi B t)}{(\pi B t)^2}(1 + n(t)) \tag{25}$$

to perform the numerical convolution to obtain the mean waveform. In this equation, $n(t)$ is a zero-mean, Gaussian

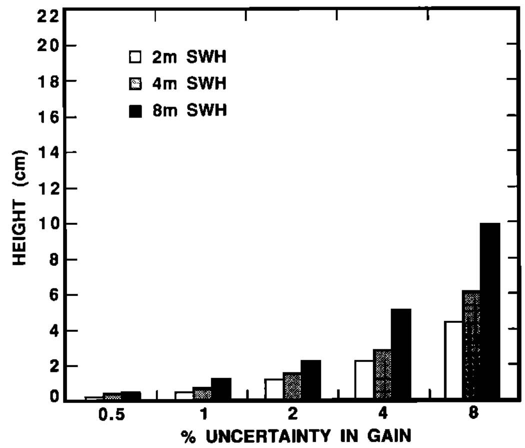

Fig. 7. Height biases (1σ) for the look-up table algorithm due to random errors in the altimeter filter gain calibration for various values of calibration accuracy.

variable whose variance can be varied at will. We then used the theoretical ptr to perform the deconvolution.

The results of this simulation showed that if the ptr was known to an accuracy of more than 5% at each time bin, the biases incurred were extremely small. This is due to the fact that even though the ptr used is noisy, since the noise is multiplicative, it roughly maintains the same side lobe structure.

On the other hand, if a ptr with different side lobe structure had been used, the estimated parameters would have been much more biased. As an example, we used the theoretical sin x/x ptr to generate mean waveforms and the measured Seasat ptr in the deconvolution for 4-m SWH and no skewness or height error. The biases induced on the estimated parameters were: 17-cm height bias; 34-cm SWH bias; 0.32 skewness bias. These results underline the necessity of using the measured altimeter ptr in the deconvolution process.

7. Examples From Seasat Data

In order to check the consistency of our results with real data, we used our algorithm on several waveform sets obtained by the Seasat altimeter. Our examples were chosen from a set of ascending repeat tracks extending from the Antarctic Circumpolar Current (latitude, −59°; longitude, 117°) to the equator at the Indian Ocean (latitude, 0°; longitude, 80°). We picked this data set because it contains a wide variety of ocean states: during the southern hemisphere winter, one usually encounters very large significant wave heights around the Antarctic Circumpolar Current, while around the equator, the significant wave height is usually small. The algorithm thus may be tested over a wide spectrum of SWHs. The rapid changes in SWH also provide an interesting set of conditions for observing the dynamical changes in the ocean skewness as the altimeter samples ocean spectra with different degrees of development. As an additional data set, we selected the hurricane Fico, since this data set has been studied by previous researchers [*Lipa and Barrick*, 1981; *Hayne*, 1980].

The Seasat data set, however, is not an ideal data set. For various reasons [*Townsend*, 1980; *Lipa and Barrick*, 1981; *Hayne and Hancock*, 1982], the Seasat tracker was noisier than the tracker of Geosat or the proposed TOPEX altimeter. Also, the calibration of the gate gains was never resolved satisfactorily (G. Hayne, private communication, 1988). This will introduce unknown biases into the estimated parameters. Furthermore, the attitude estimated by the satellite sensor does not always seem to coincide with the attitude expected from waveform analysis (G. Hayne, private communication, 1988). In spite of these reservations, the Seasat data set does represent a widely available data set which has been analyzed in the past. While it is probably not feasible to expect exact agreement with our simulation, the results should be qualitatively the same.

The largest uncertainty in the filter gains of the Seasat data set is at the leading edge of the waveform. The corrections proposed in the past [*Hayne*, 1980] have been small for this part of the waveform, and we have decided to ignore them. This implies that the parameters we estimate may suffer from small biases relative to the ocean parameters. Also, we have decided to use the attitude estimated by the spacecraft, since we feel that the uncertainty in the gain distortions of the waveform, especially the large waveform droop in the last part of the trailing edge [*Townsend*, 1980], preclude a much more accurate estimation of the mispointing from the waveform.

In order to minimize the biases in the estimated skewness, we have deconvolved waveforms averaged over 1 s. This corresponds to the Seasat geophysical data records (GDR) data rate. In order to study the trends in the behavior of the estimated parameters, we removed random noise by applying a box filter to the estimated parameters. The box filter applied to the estimated parameters was 31 s long. The corresponding ground averaging distance is approximately 200 km, which is roughly of the same order of magnitude as the size for mesoscale variability.

The results for three representative examples of the repeat tracks and for the hurricane Fico are presented in Figure 8. Examination of the estimated height error shows a marked correlation between this quantity and SWH. This effect has been noted previously both for the sensor data record (SDR) estimated height (before corrections) [*Barrick and Lipa*, 1985; *Hayne and Hancock*, 1982], and for the geophysical data record estimated height (after corrections have been applied) [*Born et al.*, 1982; *Douglas and Agreen*, 1983]. In particular, it is shown in the first two references that, for the SDR data, one should expect a tracker bias that varies from about 3% to about 5% of SWH towards the troughs of the waves. One should also expect the percentage to increase with increasing SWH. This is consistent with what is observed in our data set. (To help comparison with other sources, we note here that the height error we quote here corresponds to z_T. Hence a positive height error implies the mean ocean surface is higher than the altimeter estimate. This corresponds to a negative change on the relative height of the altimeter to the surface.)

It should be noted that the final tracker error, i.e., the one that appears on the GDR, is different from the SDR tracker error. This is due to the fact that corrections may be applied on the ground to compensate for the known biases of the altimeter tracker (e.g., attitude corrections, or SWH corrections). A large part of the tracker error is thus eliminated. However, these corrections cannot compensate for parameters which are not estimated by the altimeter (e.g., skewness biases). As we shall see below, these biases can still be quite large.

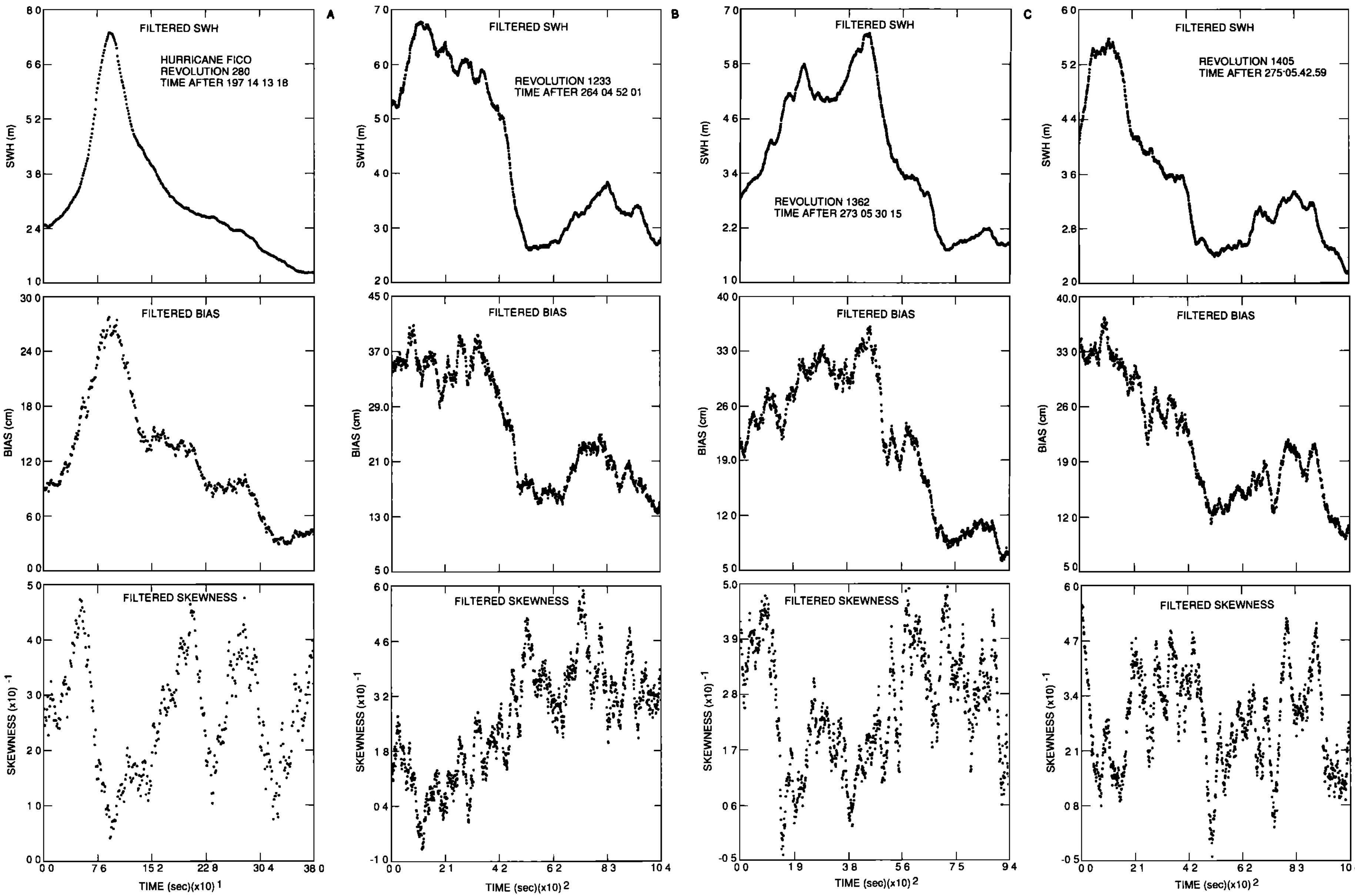

Fig. 8. Parameters estimated from Seasat altimeter 1-s-averaged waveforms for a pass over (*a*) hurricane Fico and (*b*–*d*) three typical long repeat tracks over the Indian Ocean. Note the high values of SWH near the Antarctic Circumpolar Current and the SWH dependence of the tracker error. Note also the high values which the ocean surface skewness may attain for long stretches.

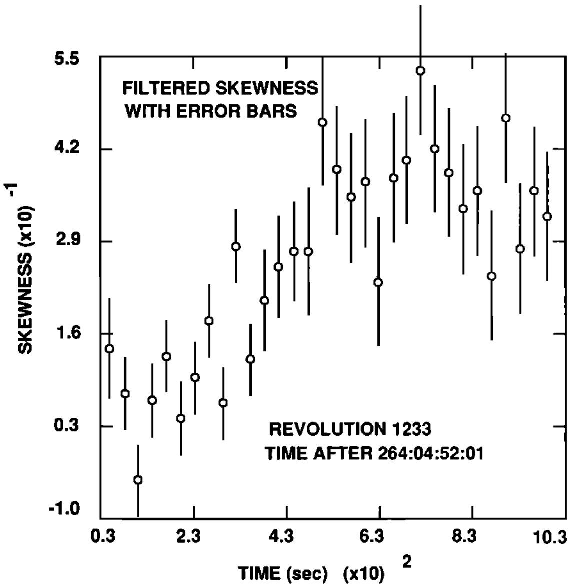

Fig. 9. A plot of every thirty-first point (independent points only) of the estimated skewness for revolution 1233 with the skewness error bars included. Note that while the long-term trend in the skewness behavior remains, the high frequency variations lie within the error bars.

A comparison of the parameters estimated over the hurricane Fico (Figure 8*a*) with the results found by previous researchers, shows a good qualitative agreement. The estimated SWH is somewhat higher at the peak of the storm (about 70 cm) in our estimate; but, for lower significant waveheight, there is substantial agreement in the estimated SWH. The height error estimated by our algorithm agrees substantially with the one estimated by Hayne (when one takes into account the effect of the filtering at the peak of the hurricane). However, it is consistently smaller than the error estimated by Lipa and Barrick. This may be due to the fact that Lipa and Barrick neglect the altimeter antenna pattern and pointing angle. There is no exact agreement in the estimated skewness between the three algorithms, although the sign and order of magnitude for the skewness is the same for all three estimates.

Since the altimeter filter gains were not accurately known, the estimated skewness is an "effective skewness," which includes the effect of waveform distortion by the filter gains. Therefore the values estimated may differ somewhat from the ocean surface skewness. It should also be mentioned that the measured skewness is the skewness of the specular point pdf (or electromagnetic skewness), not the skewness of the ocean surface pdf. If geometric optics is applicable to this scattering situation, the difference between the two skewnesses is small [*Rodríguez*, 1988]. However, there is a possibility that there may be additional differences due to unmodeled sources such as foam, wave breaking, or the modulation of small capillary waves by the larger gravity waves. Nevertheless, the behavior of the estimated skewness shows remarkable structure and features which one would expect from the true surface skewness.

For instance, the skewness estimated in all our examples is preponderantly positive. This is in agreement with the prediction of weak nonlinear wave theory [*Longuet-Higgins*, 1963]. The magnitude of the skewness seems to vary between a minimum of 0 and a maximum of about 0.4. Its average value seems to be between 0.2 and 0.3. This is also consistent with the limited set of observations by Kinsman as quoted by *Longuet-Higgins* [1963].

The estimated skewness also exhibits coherent long wavelength trends in all cases. An especially salient example of long-range structure is present in the estimated skewness for revolution 1233, where a marked change in the skewness value coincides with a change in the value of SWH. This indicates that the estimated skewness reflects a geophysical parameter, since algorithm noise would not exhibit this long-term coherence.

In addition to these long-term trends, the skewness estimates in Figure 8 seem to exhibit a great deal of internal structure. That this structure is artificial, however, can be seen if we plot only independent points (i.e., every thirty-first point) together with their error bars. Figure 9 presents an example for revolution 1233. The error bars are obtained by scaling the standard deviations in Table 5*c* by $1/31^{1/2}$ to take into account the noise reduction due to averaging. As can be seen, only the long-wavelength trends are real, while the high-frequency variations lie within the error bars.

The estimated skewness is not strongly correlated with wave sea state. Figures 8*a* and 8*b*, for instance, show situations where high sea state corresponds to low skewness. Figures 8*c* and 8*d*, on the other hand, show that high sea states can also have high skewness values. The same type of observation can be made for low sea states. This implies that the estimated skewness is a parameter independent of the estimated SWH, and thus not a SWH dependent bias in the algorithm. This is the type of bias one would observe if the estimated skewness were merely an artifact due to the filter gains. A formal correlation analysis of the estimated parameters also shows that their correlation is not

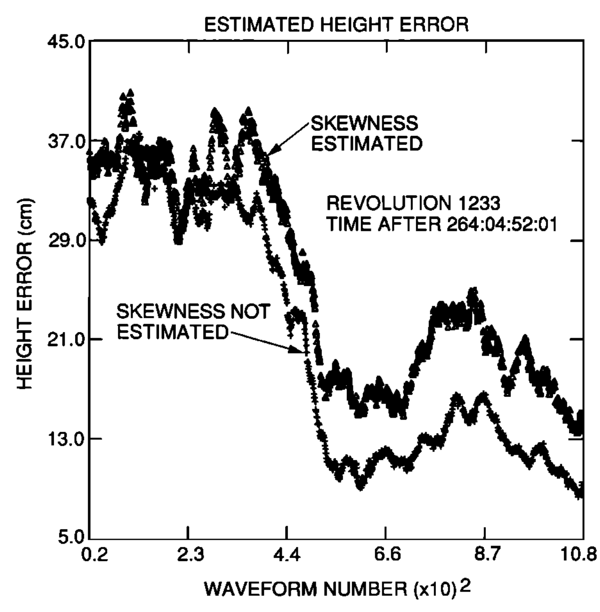

Fig. 10. A comparison of the estimated height error when skewness is and is not estimated by the deconvolution algorithm for revolution 1233. Notice that for the higher values of SWH, when the skewness is small, the two estimates coincide substantially. However, for the lower SWH, which has higher skewness, there is a centimeter level difference between the two estimates. The difference is of the same magnitude as expected from the measured skewness. This type of bias is of great importance in the accuracy of high-precision ocean altimeters, such as TOPEX.

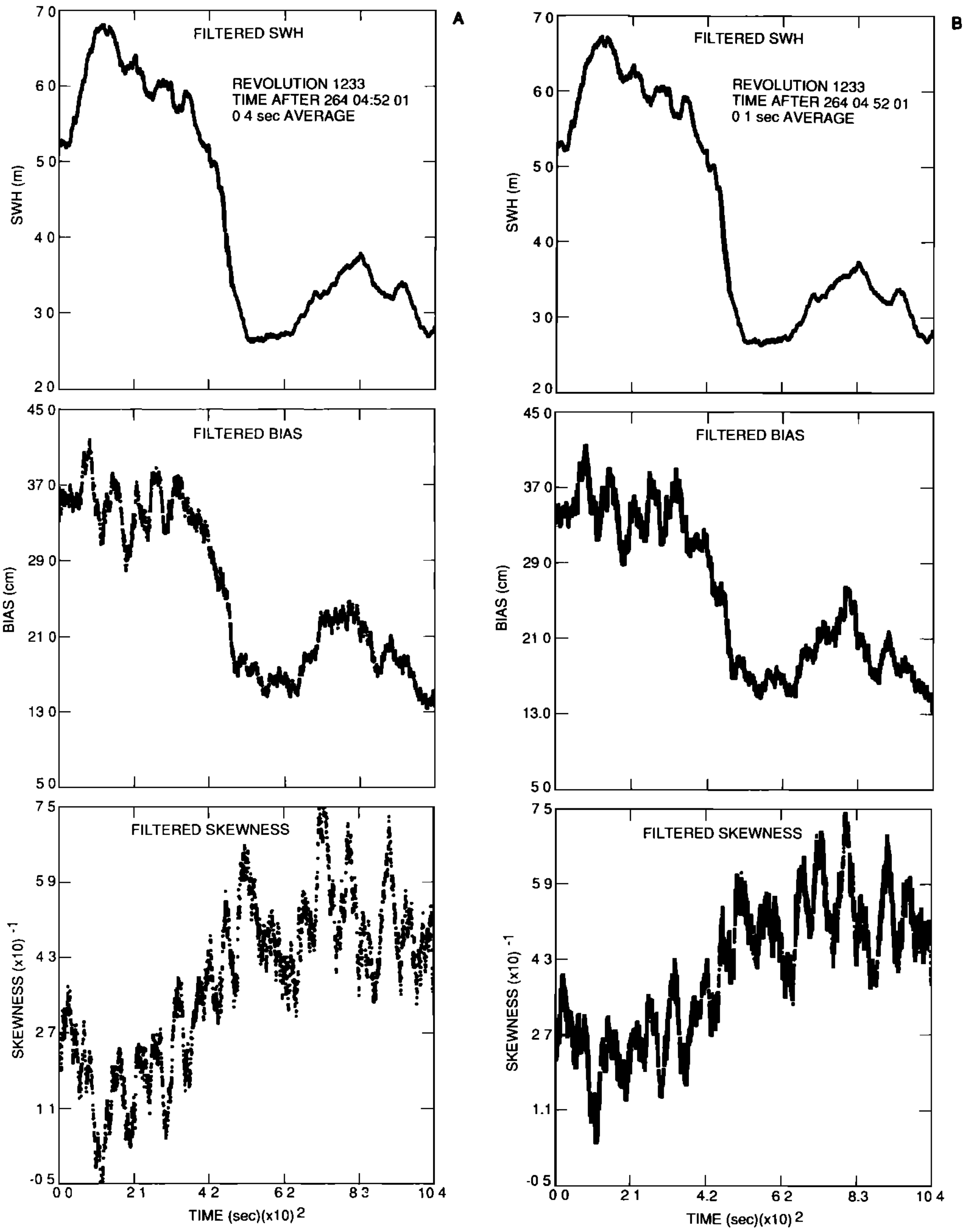

Fig. 11. Variability of the estimated parameters as a function of the number of waveforms averaged for the data in revolution 1233. (*a*) Parameters estimated from 0.1-s-averaged waveforms. (*b*) Parameters estimated from 0.4-s-averaged waveforms. These figures should be compared with Figure 8*b*, which shows the parameters estimated from 1-s-averaged waveforms for revolution 1233. The three data sets are filtered to the same resolution.

strong. There does seem to be a correlation between high skewness values and the transition regions between different values of SWH. However, these are not the only regions where high skewness seems to occur. A more detailed study of the properties of ocean skewness will be deferred to a subsequent paper.

The high values and long wavelength changes of the skewness found in this study have important consequences for high-precision ocean altimeters such as TOPEX. *Srokosz* [1986] and *Rodríguez* [1988] showed that the skewness bias can be approximated by

$$\text{bias} = \lambda \frac{\text{SWH}}{24} \tag{26}$$

For a skewness of $\lambda = 0.3$, this implies a bias of about 1.2% of SWH, which is comparable with the centimeter level accuracy required for this altimeter. As an example of the consequences of not estimating skewness, we present in Figure 10 a comparison of the estimated height error when skewness is and is not estimated for the data in revolution 1233. As can be seen, in the areas of high skewness, there is a consistent centimeter level difference between the two estimates.

To examine the assumption that waveforms could be averaged in order to reduce biases in the estimated parameters while maintaining the same trends, we estimated the parameters from revolution 1233 for unaveraged waveforms, and

TABLE 6. Seasat Estimated Data Noise

Average SWH, m	σ_h, cm	σ_{SWH}, cm	σ_λ	Start Time	End Time	Revolution
1.8	5.2	20	0.52	197:14:17:53	197:14:19:31	0280
2.0	5.9	20	0.55	273:05:41:22	273:05:46:16	1362
2.0	5.9	21	0.55	258:05:30:01	258:05:40:47	1147
2.5	7.2	24	0.48	279:06:05:11	279:06:10:05	1448
2.7	7.0	24	0.47	276:05:51:38	276:06:00:37	1405
2.8	7.3	25	0.49	267:05:15:52	267:05:22:24	1276
3.1	8.1	28	0.46	264:05:01:29	264:05:09:39	1233
3.3	7.7	33	0.44	270:05:20:07	270:05:23:43	1319
3.7	10.0	36	0.51	276:05:46:44	276:05:50:00	1405
4.1	9.6	43	0.46	267:05:04:27	267:05:09:20	1276
4.9	8.9	43	0.38	261:04:38:56	261:04:41:51	1190
5.3	10.4	46	0.37	276:05:44:17	276:05:45:55	1405
5.4	11.2	45	0.39	258:04:26:12	258:04:31:54	1147
5.6	11.8	43	0.37	273:05:34:50	273:05:38:06	1362
6.0	12.4	58	0.39	264:04:54:37	264:04:57:43	1233
8.2	17	67	0.47	261:04:44:57	261:04:46:35	1190

Times are in days: hours: minutes: seconds.

waveforms averaged for 0.1, 0.4, and 1 s. We then smoothed the data with a 31-s box filter to compare the trends. The results for 0.1- and 0.4-s averaging are shown in Figure 11 (the 1-s averaging result was shown in Figure 8). As can be seen, the skewness for 0.1-s waveforms is significantly biased, as expected. On the other hand, both SWH and height errors are consistent for the three averaging times.

In order to obtain an estimate of the noise in our estimates with that predicted by our simulation (Table 5), we selected areas where the significant waveheight remained approximately constant for many data points (in order to allow the tracker to achieve a steady state behavior) and calculated the standard deviation of the data about the 31-s-averaged data. In our limited data set it was not possible to find areas of persistently large SWH, since this condition does not usually exist over long distances. Nevertheless, we followed the same procedure for these cases (approximately for SWH higher than 3 m) to get a ballpark estimate of the noise. The results are presented in Table 6. Notice that the standard deviation we obtain for the height error should correspond to the rss sum of the tracker jitter and the algorithm noise. Also, for high SWH, the average SWH shown is often significantly smaller than the peak SWH in that data segment.

Comparing these results with the ones obtained by the simulation, we observe good agreement for the cases of low SWH. For the high-SWH cases, there is order of magnitude agreement between the two results, but the actual data are somewhat noisier, especially in the estimation of SWH. We believe this is due to the dynamic behavior of the tracker. Additional tracker jitter and drift will cause the size of the leading edge to fluctuate more strongly than our simulation allowed for.

8. Summary and Conclusions

In this paper we presented a detailed study of the properties of the deconvolution method of estimating ocean surface parameters. Our main result was the selection of a "best" method of deconvolution to reduce the noise in the estimated parameters. This method, which we dub the "power deconvolution" method, was then extensively tested in a Monte Carlo simulation to determine its performance characteristics under various conditions. We found that the height estimated using this algorithm was unbiased by the ocean surface skewness. This is the main advantage of this algorithm over the ones used for the Seasat and Geosat altimeters. This algorithm has the additional advantage over previous parameter estimation algorithms [*Hayne and Hancock*, 1982] that the fitting function is a simple analytic function. This simplifies and expedites the fitting process, since numerical derivatives do not have to be calculated. The running time of our algorithm was shown to be under 1 s for nonoptimized code on a micro-VAXII computer. We expect that this time can be reduced to close to real time in the future. This may have important implications in the ground processing of the data from the TOPEX altimeter.

On the other hand, the algorithm was shown to be approximately 2 times noisier in its height estimate than the traditional look-up table algorithm. It is also more sensitive to filter gain noise. Hence we conclude that one is justified in using this algorithm only if the specular point pdf skewness is greater than 0.1. Our results from the Seasat altimeter seem to indicate that this is often the case. However, this cannot be judged a conclusive proof, since this altimeter was subject to various instrument problems and was never fully calibrated. We are presently conducting similar studies using the Geosat altimeter data and hope to soon be able to better answer this question.

The estimated skewness was shown to be biased when estimated from 0.1-s waveforms. However, when longer averages were taken, the biases in this parameter decreased. The noise level of the estimated SWH was shown to be much smaller than the TOPEX performance requirement. The estimated skewness, on the other hand, was shown to be quite noisy, so that reliable estimates can be obtained only by averaging over long time intervals. These time intervals, however, are smaller than the typical scale of mesoscale variability.

In order for the algorithm to work, the altimeter attitude and point target responses need to be known a priori. However, we showed that the algorithm was quite robust when errors in the estimates of these quantities were present. On the other hand, it was shown that the estimated parameters were sensitive to the calibration of the filter gains. We derived requirements on the accuracy of these gains.

Finally, we compared our simulation results with data from the Seasat altimeter and found good agreement. We also observed the same SWH dependent height biases which had been previously observed by many researchers. The most intriguing part of the results from real data was the magnitude and behavior of the skewness. The magnitude was found to be large enough that it would be a significant contributor to the height error budget if it were not estimated. As was mentioned before, if this result also holds for better calibrated altimeters, it will have important consequences for the high-accuracy TOPEX altimeter. It was also observed that the skewness showed long-wavelength variations which were not obviously correlated with SWH. Further research on the characterization of this behavior is currently in progress.

APPENDIX: SPECTRAL FILTERING

One can find an orthogonal transformation matrix O such that the symmetric matrix $\Gamma = MM^T$ can be written as

$$\Gamma = O\Lambda O^T$$

where Λ is diagonal and its elements are the eigenvalues of Γ, and

$$OO^T = O^TO = 1$$

Then the Lanczos inverse of Γ is given by

$$\Gamma_L^{-1} = O\Lambda_L^{-1}O^T \tag{27}$$

where Λ_L^{-1} is the matrix one obtains by replacing the nonzero elements of Λ by their inverses. It can be shown that the Lanczos inverse provides the least squares solution of a singular matrix equation.

Using the Lanczos inverse, one can give the solution of equation (9) as follows

$$x = M^T\Gamma_L^{-1}y \tag{28}$$

It is easy to verify that if M is square and not singular, this corresponds to the matrix inverse. To obtain the spectral representation of the solution, introduce the orthogonal matrix

$$\Psi = \Lambda^{-1/2}O^TM \tag{29}$$

whose columns constitute a basis for expanding the solution. The expansion weights can be shown to be given by the vector

$$w = \Lambda^{-1/2}O^Ty \tag{30}$$

such that

$$x = \Psi^Tw \tag{31}$$

It can be seen from this last expression that in the presence of noise, if $\lambda_j \ll \lambda_{max}$, the noise will be magnified disproportionately due to the large relative value of the expansion weight. The idea of spectral filtering is to discard all vectors in the spectral expansion whose weight is such that the associated eigenvalues satisfies the condition $(\lambda_j/\lambda_{max})$ < threshold, where λ_{max} is the largest eigenvalue and the threshold is a preset constant.

Acknowledgments. We would like to thank L. L. Fu, F. K. Li, and C. Y. Chi for comments on the work described in this paper. We would also like to thank an anonymous reviewer for his comments regarding the estimated skewness. The research described in this paper was performed by the Jet Propulsion Laboratory, California Institute of Technology, under contract with the National Aeronautics and Space Administration.

REFERENCES

Applied Physics Laboratory, Geosat-A data users/ground system ICD, *Doc. 792-9510*, Johns Hopkins Univ., Laurel, Md., 1985.

Barrick, D. E., Remote sensing of sea state by radar, in *Remote Sensing of the Troposphere*, vol. AP-16, edited by V. E. Derr, chap. 12, U.S. Government Printing Office, Washington, D. C., 1972.

Barrick, D. E., and B. J. Lipa, Analysis and interpretation of altimeter sea echo, in *Satellite Oceanic Remote Sensing, Adv. in Geophys.*, vol. 27, edited by B. Saltzman, pp. 61–100, 1985.

Barrick, D. E., P. M. Woiceshyn, J. C. Wilkerson, G. H. Born, and D. B. Lame, Seasat Gulf of Alaska Workshop II report, *JPL Intern. Doc. 622-107*, Jet Propul. Lab., Pasadena, Calif., 1980.

Benedict, T. R., and G. W. Bordner, Synthesis of an optimal set of radar track-while-scan smoothing equations, *IRE Trans. Autom. Control, AC-7*, 27–32, 1962.

Berger, T., Satellite altimetry using ocean backscatter, *IEEE Trans. Antennas Propag., AP-20*, 295–309, 1972.

Born, G. H., M. A. Richards, and G. W. Rosborough, An empirical determination of the effects of sea state bias on Seasat altimetry, *J. Geophys. Res., 87*(C5), 3221–3226, 1982.

Born, M., and E. Wolf, *Principles of Optics*, 6th ed., Pergamon, Elmsford, N.Y., 1980.

Brown, G. S., The average impulse response of a rough surface and its applications, *IEEE Trans. Antennas Propag., AP-25*, 67–74, 1977.

Douglas, B. C., and R. W. Agreen, The sea state correction for GEOS 3 and Seasat satellite altimeter data, *J. Geophys. Res., 88*(C3), 1655–1661, 1983.

Hayne, G. S., Radar altimeter mean return waveforms from near-normal-incidence ocean surface scattering, *IEEE Trans. Antennas Propag., AP-28*, 687–692, 1980.

Hayne, G. S., and D. W. Hancock, Sea-state related altitude errors in the Seasat radar altimeter, *J. Geophys. Res., 87*(C5), 3227–3231, 1982.

Howard, S. J., Fourier spectrum continuation, in *Deconvolution With Applications in Spectroscopy*, edited by P. A. Jansson, pp. 261–288, Academic, San Diego, Calif., 1984.

Jansson, P. A., (Ed.), *Deconvolution: With Applications in Spectroscopy*, Academic, San Diego, Calif., 1984.

Jet Propulsion Laboratory, NASA, and Centre National d'Etudes Spatiales, TOPEX/POSEIDON mission description, Rep. *1633-5*, Rev. B, Jet Propul. Lab., Calif. Inst. of Technol., Pasadena, Dec. 1985.

Lanczos, C., *Linear Differential Operators*, Van Nostrand-Reinhold, New York, 1961.

Lipa, B. J., and D. E. Barrick, Ocean surface height-slope probability density function from Seasat altimeter echo, *J. Geophys. Res., 86*(C11), 10,921–10,930, 1981.

Longuet-Higgins, M. S., The effect of nonlinearities on statistical distributions in the theory of sea waves, *J. Fluid Mech., 17*, 459–480, 1963.

MacArthur, J. L., Seasat-A radar altimeter design description, *Doc. SDO-5232*, Appl. Phys. Lab., Johns Hopkins Univ., Laurel, Md., Nov. 1978.

Marquardt, D. W., An algorithm for least-squares estimation of nonlinear parameters, *J. Soc. Ind. Appl. Math., 11*, 431–441, 1963.

Parker, R. L., Understanding inverse theory, *Annu. Rev. Planet. Sci.*, 35–64, 1977.

Phillips, O. M., The dynamics of the upper ocean, 2nd ed., Cambridge University Press, New York, 1977.

Press, W. H., B. P. Flannery, S. A. Teukolsky, and W. T. Vetterling, *Numerical Recipes*, Cambridge University Press, New York, 1986.

Priester, R. W., and L. S. Miller, Estimation of significant wave height and wave height density function using satellite altimeter data, *J. Geophys. Res.*, *84*(B8), 4021–4025, 1979.

Rodríguez, E., Altimetry for non-Gaussian oceans: Height biases and parameter estimation, *J. Geophys. Res.*, *93*(C11), 14,107–14,120, 1988.

Srokosz, M. A., On the joint distributions of surface elevation and slopes for a nonlinear random sea, with applications to radar altimetry, *J. Geophys. Res.*, *91*(C1), 995–1006, 1986.

Twomey, S., On the solution of Fredholm integral equations of the first kind by the inversion of the linear system produced by quadrature, *J. Assoc. Comput. Mach.*, *10*, 97–101, 1963.

Townsend, W. F., An initial assessment of the performance achieved by the Seasat-1 radar altimeter, *IEEE J. Oceanic Eng.*, *OE-5*, 80–92, 1980.

Ulaby, F. T., R. K. Moore, and A. K. Fung, *Microwave Remote Sensing*, vol. 2, Addison-Wesley, Reading, Mass., 1982.

Walsh, E. J., Pulse-to-pulse correlation in satellite radar altimeters, Radio Sci., *17*(4), 786–800, 1982.

Walsh, E. J., et al., Electromagnetic bias of 36-GHz radar altimeter measurements of MSL, *Mar. Geod.*, *8*(1–4), 265–296, 1984.

Wingham, D. J., Onboard correction of mispointing errors in satellite altimeter returns, *IEEE J. Oceanic Eng.*, *13*(2), 77–81, 1988.

E. Rodríguez and B. Chapman, Jet Propulsion Laboratory, California Institute of Technology, 4800 Oak Grove Drive, Pasadena, CA 91109.

(Received November 23, 1988;
accepted January 9, 1989.)